133

Egypt. J. Chem. **Vol. 67** No. 3 pp. 357- 377 (2024)

Egyptian Journal of Chemistry

Anti-Alzheimer Activity and UHPLC-MS Based Molecular Networking of *Pseudobombax ellipticum* Cultivars Coupled to Multivariate Data Analysis and In Silico Molecular Docking

Ahmed S. Mohamed[1*], Osama G. Mohamed [1,2,5], Ali M. El Shamy[1], Fatma S. El Sakhawy[1], Ahmed A. Al-Karmalawy[3,4], Ashootosh Tripathi[2,5] and Rania A. El Gedaily[1].

[1] *Department of Pharmacognosy, Faculty of Pharmacy, Cairo University, Kasr Al-Aini St., Cairo 11562, Egypt.*
[2] *Natural Products Discovery Core, Life Sciences Institute, University of Michigan, Ann Arbor, MI 48109, USA.*
[3] *Department of Pharmaceutical Chemistry, Faculty of Pharmacy, Horus University-Egypt, New Damietta 34518, Egypt.*
[4] *Pharmaceutical Chemistry Department, Faculty of Pharmacy, Ahram Canadian University, 6th of October City, Giza 12566, Egypt.*
[5] *Department of Medicinal Chemistry, College of Pharmacy, University of Michigan, Ann Arbor, MI 48109, USA.*

Abstract

Pseudobombax ellipticum (Kunth) Dugand and the cultivar alba Hort. are members of family Bombacaceae. Their chemical composition is still under investigation. The current study aimed to investigate their chemical compositions, exploring the variations between organs and or cultivars and *in vitro* screening of the anti-Alzheimer activity of their ethanolic extracts against butyryl and acetyl cholinesterases enzymes. Primary phytochemical screening revealed the presence of secondary metabolites of mainly flavonoids, tannins, and terpenoids classes. Total phenolics and flavonoids were quantified in both cultivars; leaves, bark, and flowers as mg gallic acid equivalent /gm extract and mg rutin equivalent/gm extract, respectively. Metabolic profiling of leaves, bark and flowers of both cultivars *via* UHPLC-HRMS in negative and positive modes resulted in the identification of 89 compounds of different classes, including simple phenols, flavonoids, fatty amides and alcohols, triterpenes, fatty acids, esters, and triacylglycerols. All of the identified compounds are reported for the first time in *Pseudobombax ellipticum*. Feature-based Molecular Networking (FBMN) demonstrated the different phytochemical classes and highlighted the major compounds in each class. Principal component analysis (PCA), hierarchical clustering analysis (HCA), and orthogonal partial least squares-discriminant analysis (OPLS-DA) explored the variance between organs and or cultivars and detected the abundant and unique compounds in each organ. Acetyl and butyryl cholinesterases inhibitory activities of both cultivars; leaves, bark, and flowers were screened at 10 and 100 μg/mL using donepezil as a positive control. All extracts showed more than 50% acetyl cholinesterase inhibitory activity at 100μg/mL and did not inhibit butyryl cholinesterase up to 100μg/mL. Furthermore, selected identified compounds were subjected to a molecular docking study that showed the highly binding affinity of most of the examined compounds towards the acetyl cholinesterase target. These results revealed the chemical richness of *Pseudobombax ellipticum* cultivars and their probability of managing several health problems.

Keywords: UHPLC-HRMS, metabolite profiling, anti-Alzheimer activity, *Pseudobombax ellipticum*, molecular networking, multivariate data analysis.

1. Introduction

Family Bombacaceae is a group of flowering plants comprising ca. 28 genera and 304 species[1][2]. Within this family, *Pseudobombax ellipticum* is native to South America and had traditionally been used to treat respiratory disorders, fever, and

Concerning the chemical composition and biological activities of *P. ellipticum* and the *Pseudobombax*

_____

genus, limited studies are available. The cortex extracts of *P. ellipticum* obtained using water and ethanol demonstrated significant antioxidant activity[5]. Additionally, stem bark yielded β-lupeol, which exhibited a potential gastro-protective effect[6]. Recently, its flowers were reported to exhibit potential anti-sickling activity against sickle cell anemia, with 8 anthocyanins identified for the first time using LC/MS[7]. Furthermore, phenolic compounds, including flavonoids, proanthocyanidins, and catechins were identified in the stem bark extract of *Pseudobombax marginatum* Robyns using spectroscopic techniques [8].

Classical approaches in drug discovery have been expedited recently by chemoinformatic tools such as GNPS and multivariate data analysis. The Global Natural Products Social Molecular Networking (GNPS) infrastructure employs feature-based molecular networking (FBMN) as tool that further aids in identification of metabolites based on its tandem mass spectral datasets and expedite drug discovery[9]. Further, multivariate data analysis allows for samples' classification, identification of discriminating metabolites and correlation between bioactivity and metabolite profile[9].

Alzheimer's disease (AD) is the most common form of dementia and is a significant global health concern that necessitates discovering for new drugs aided by modern bioinformatics tools in drug discovery[10][11]. AD is a degenerative brain disorder characterized by memory disturbances, personality changes, and sleep abnormalities[10]. The FDA has approved synthetic medications as acetylcholinesterase inhibitors (AChEIs), including drugs like donepezil, tacrine, and galantamine, for treating AD. However, these synthetic drugs have been associated with various adverse effects[12], warranting for the development of more safe and effective drugs from natural sources[13].

Interestingly, the ethanol and defatted ethanol extracts of *Durio zibethinus* L. fruits (Bombacaceae) have demonstrated significant activity against AD asides from their potential antioxidant, anti-acetylcholinesterase, and nerve protective effects[14].

The current study employed ultra high performance liquid chromatoghraphy high resolution mass spectrometry (UHPLC-HRMS) combined with molecular networking (GNPS –MN) and multivariate data analysis to further investigate *P. ellipticum* metabolite profile in a holistic manner. In addition, in-vitro screening of the anti-Alzheimer's activity of different organs from each *P. ellipticum* cv. against butyryl and acetylcholinesterases enzymes was performed as screening tool. Furthermore, binding affinity of the major and discriminating identified compounds towards the acetylcholinesterase target was investigated to aid identify of best chemicals that have yet to be tested individually in future studies post isolation.

2. Material and methods
2.1. Plant material

The three organs (leaves, bark and flowers) of the studied cultivars were collected from Mostafa El Abed botanical garden, from Sept. 2019 to May 2020. Dr. Mohamed El Gibali, Senior Botanist & Consultant at Orman Botanic Garden, Giza, Egypt, kindly identified the plant. A vouchered specimen of the plant, with serial number (20.09.2022) was kept at the herbarium of the Pharmacognosy Department, Faculty of Pharmacy, Cairo University. The collected leaves and bark plant materials were, separately, air-dried in shade for 3 weeks and dried materials were ground into powder..

Preparation of crude extracts
Aliquots of leaves and bark powders of the studied cultivars (20 g, each) were extracted with 70% ethanol (200 × 3 times). In the case of flower extracts, fresh flowers (50 g) from each cultivar were dissected by scissors to small pieces and separately extracted with 70% ethanol (200 × 3 times). All extracts were evaporated under reduced pressure in a rotary evaporator (Büchi, Switzerland) at a temperature of 60°C, yielding 10, 9.5, 8, 7, 6 and 5.6% w/w for PR and PW leaves (LR and LW), bark (BR and BW) and flowers (FR and FW), respectively (expressed as the weight of the extract relative to the weight of the initial plant material)[15][16].

2.2. Preliminary phytochemical screening
All extracts under study were screened for the presence or absence of most secondary metabolites using standard phytochemical procedures and tests[17]. Molish's test, alkaline reagent test, ferric chloride test, salkowski's test, froth test, mayer's and dragendroff's tests, borntrager's test and baljet test were used for the detection of carbohydrates, flavonoids, tannins, sterols and triterpenes, saponins, alkaloids, anthraquinones and cardiac glycosides, respectively.

2.3. Determination of total phenolic and flavonoid contents
Total phenolic (TPC) and total flavonoid (TFC) contents of tested samples were determined spectrophotometrically using Folin–Ciocalteu and Aluminum chloride assays, respectively. For total

_____

phenolic content (TPC), a stock solution of 1 mg/ml of gallic acid in methanol was prepared as the standard. Seven serial dilutions were made at concentrations of 1000, 800, 600, 400, 200, 100, and 50 μg/ml while in case of total flavonoid content (TFC), a stock solution of 1 mg/ml of rutin in 100% methanol was prepared as the standard, and seven serial dilutions were made at concentrations of 1000, 600, 400, 200, 100, 50 and 10μg/ml. The tested samples were prepared in a 4 mg/ml concentration in methanol. The absorbance of the color produced was measured at 630 nm for TPC [18] and 415 nm for TFC [19] on a microplate reader (FluoStar Omega, bmg labtech, Ortenberg, Germany). Six replicates of the 7 standards and 6 samples were pipetted into the plate wells. The average of the absorbance readings of the 6 replicates for gallic acid and rutin standards were recorded and calibration curves were established. The TPC and TFC were detected by substituting the linear regression equation.

2.4. UHPLC-HRMS QTOF-MS/MS profiling of the crude extracts

An Agilent LC–MS system composed of an Agilent 1290 Infinity II UHPLC coupled to an Agilent 6545 ESI-Q-TOF-MS in both negative and positive modes was used to obtain Ultra-high-performance liquid chromatograms[20][21]. Aliquots (1 µL) of ethanolic extracts (5 mg/mL in MeOH) were analyzed on a Kinetex phenyl-hexyl (1.7 µm, 2.1 × 50 mm) column. Isocratic elution of 90% A (A: 100% H_2O + 0.1% formic acid) for 1 min followed by 6 min linear gradient elution to 100% B (95% MeCN + 5% H_2O + 0.1% formic acid) with a flow rate of 0.4 mL/min followed by 2 min isocratic elution with 100% B. ESI conditions were set with the capillary temperature at 320 °C, source voltage at 3.5 kV and a sheath gas flow rate of 11 L/min. Ions detected in the full scan at an intensity above 1000 counts at 6 scans/s, with an isolation width of 1.3 ~m/z, a maximum of 9 selected precursors per cycle and using ramped collision energy (5× m/z/100 + 10 eV). Purine $C_5H_4N_4$ [M + H]+ ion (m/z 121.0509) and hexakis (1H,1H,3H-tetrafluoropropoxy)-phosphazene $C_{18}H_{18}F_{24}N_3O_6P_3$ [M + H]+ ion (m/z 922.0098) were used as internal lock masses for positive mode while TFA $C_2HF_3O_2$[M − H]− ion (m/z 112.9856) and hexakis (1H,1H,3H-tetrafluoropropoxy)-phosphazene $C_{18}H_{18}F_{24}N_3O_6P_3$ [M + TFA − H]− ion (m/z 1033.9881) were used as internal lock masses for negative mode. Using MSConvertGUI, the mzXML files were imported and processed with MZmine 2 v2.53[22] with the following workflow: (i) Mass Detection: MS1 noise level, 1E3; MS2 noise level, 1E2. (ii) ADAP chromatogram builder: MS-level, 1; min group size in no. of scans, 5; group intensity threshold, 2E3; min highest intensity, 2E3;

m/z tolerance, 0.00 m/z or 10 ppm. (iii) Chromatogram deconvolution: Local minimum search algorithm; m/z range for MS2 scan pairing, 10 Da; RT range for MS2 scan pairing, 0.5 min. (iv) Isotopic peaks grouper: m/z tolerance, 0.00 m/z or 10 ppm; RT tolerance, 0.1 min; maximum charge, 3; representative isotope, most intense. (v) peak alignment: Join aligner; m/z tolerance, 0.00 m/z or 10 ppm; weight for m/z, 75; RT tolerance, 0.1 min; weight for RT, 25. (vi) Peak list rows filter: Only features with accompanying MS2 data and their retention time between 0 and 9.0 min were kept. The resulting feature lists were exported to the GNPS-compatible format, using the dedicated "Export for GNPS" built-in options.

2.5. GNPS feature-based molecular MS/MS network

Using the Feature-Based Molecular Networking (FBMN) workflow (version release_28.2) on GNPS, molecular network was created[23]. In an mgf file, the resulting aligned list of features was exported besides their feature quantification table in csv format. Sample metadata table was also prepared in text (Tab delimited) format. The mgf file, the feature quantification table and the metadata table were uploaded onto the FBMN page of GNPS. The precursor and fragment ion masses tolerance were both set to 0.02 Da. Edges of the molecular network were filtered to have a cosine score above 0.65 and more than 4 matched peaks between the connected nodes. The edges between two nodes were kept in the network and only if each of the nodes appeared in each other's respective top 10 most similar nodes. The size of clusters in the network was set to a maximum of 100 and a maximum shift 500 Da between precursors. The molecular networks were visualized using Cytoscape 3.9.1.[24]. The link for GNPS jobs that were created is (https://gnps.ucsd.edu/ProteoSAFe/jobs.jsp#%7B%22table_sort_history%22%3A%22create_time_millis_dsc%22%7D).

2.6. Multivariate data analysis

Principal component analysis (PCA), hierarchical clustering analysis (HCA) and orthogonal partial least squares-discriminant analysis (OPLS-DA) were performed on the MS-data (The feature quantification table in csv format) using MetaboAnalyst 5.0, noticing that all samples were analyzed in triplicates. By analyzing the PCA Bi-plot and OPLS-DA S-plot, abundant and unique compounds were subsequently identified. The OPLS-DA model performance was assessed by monitoring R2 and Q2 values indicating for the goodness of model fit and the degree of model predictability, respectively. S-plot was declared with covariance (p)

_____

and correlation (pcor). All variables were Pareto-scaled and mean-centered[25][26].

2.7. *In-vitro* acetyl and butyryl cholinesterases assays

Using Ellman's microplate assay with slight modifications, the tested samples' acetyl and butyrylcholinesterases inhibitory activity were screened at 10 and 100 µg/mL[27][28]. A microplate reader (FluoStar Omega, bmg labtech, Ortenberg, Germany) was used for absorbances measurement at 412 nm after 30 min of initiation of enzymatic reaction. Each test was conducted in triplicate. Donepezil was used as a positive control. The results were expressed as the percentage inhibition (%) represented as means ± SD.

2.8. Molecular docking study

The identified compounds from different organs of *P. ellipticum* cultivars were docked against the active pocket of AChE using the co-crystallized donepezil as a reference standard. The AutoDock Vina software [29] was used and the Chimera-UCSF one [30] was applied for visualization. This was done to investigate the binding affinity of the examined compounds toward the AChE target. First, the identified candidates were extracted from PubChem, introduced individually into the drug design program working window, corrected, and energy minimized [31]. The target AChE was downloaded from (https://www.rcsb.org/structure/4EY7, Protein Data Bank), opened into the working window, corrected, 3D hydrogenated, and energy minimized [32]. A general docking process was carried out and the best pose for each tested compound based on the score, RMSD (Root Mean Square Deviation), and the binding mode was selected [33]. Moreover, a validation process was carried out by redocking the co-crystal donepezil within its binding pocket and a valid performance was confirmed by obtaining low RMSD value (< 2 Å) and an acceptable binding mode as well [34],[35].

3.   Results and Discussion
3.1.   Phytochemical screening

Preliminary phytochemical screening revealed the presence of secondary metabolites, mainly carbohydrates, flavonoids, tannins, and terpenoids, while other secondary metabolites like saponins, alkaloids, anthraquinones, and cardiac glycosides were absent.

3.2.   Total phenolic and flavonoid contents

Total phenolics expressed as mg gallic acid equivalent/gm extract were detected at 81.72 ± 5.39, 73.29 ± 4.55, 36.08 ± 2.55, 99.70 ± 5.85, 163.9 ± 6.05 and 43.13 ± 4.2 mg/g extract in LR, LW, BR, BW, FR and FW, respectively. Likewise, total flavonoids level expressed as mg rutin equivalent/gm extract were detected at 65.66 ± 2.2, 24.27 ± 2.24, 6.35 ± 0.457, 7.29 ± 0.57, 71.92 ± 4.0, and 34.5 ± 3.8 mg/g extract in LR, LW, BR, BW, FR and FW, respectively. FR showed the higher phenolic and flavonoid contents.

3.3.   Metabolome profiling of *P. ellipticum* crude extracts *via* UHPLC- MS based molecular networking

Metabolite profiling of different organs of both cultivars under investigation was carried out via UHPLC-ESI-QTOF-MS/MS (*n = 3*) in negative and positive modes, in an attempt to identify valuable metabolites with intended bioactivity. The obtained respective base peak chromatograms (BPCs) of the different extracts revealed significant differences (Fig. 1 & Suppl. Fig.S1), suggesting that each organ prioritizes the recovery of specific primary or secondary metabolites. Further, ESI- QTOF-HRMS/MS and molecular networking were used to explore metabolite structures. Based on their retention times, molecular formulae, and fragmentation patterns, metabolites were tentatively annotated compared to earlier reported data aided with the mass spectrometry-based molecular networking annotation, GNPS spectral library search, and Sirius[36].

In total, 89 compounds were annotated in both positive and negative mode (Tables 1), belonging to different classes, including simple phenols and flavonoids, fatty amides and alcohols, triterpenes, and fatty acids, esters, and triacylglycerols. The presence or absence of the identified compounds in each extract was declared in (Table 1). It's noteworthy that this study is the first to explore the detailed phytochemical comparative analysis of the currently investigated *P. ellipticum* cultivars and all of the identified compounds are reported for the first time in *Pseudobombax ellipticum*. Global Natural Products Social (GNPS) molecular networking was employed to analyze HRMS/MS data. Visual analysis of MS/MS data via molecular networking (MN) enabled annotation of metabolites, together with highlighting discriminating features between dissimilar samples; LR, LW, BR, BW, FR and FW. Therefore, further molecular networking, developed using GNPS system, was imported to Cytoscape 3.9.1 to visualize MS/MS data. Within the network, each node correlates to one consensus MS/MS spectrum, representing precursor ion mass (m/z). Nodes showing common fragmentation spectra are

_____

_____

connected with edges. Each network was displayed as pie chart with grey, orange, pink, yellow, green and blue colors representing distribution of the precursor ion intensity in the LR, LW, BR, BW, FR and FW, respectively. The node size expressed the precursor ion intensity. Two molecular networks were separately displayed for both cultivars under investigation in negative and positive ionization modes (Fig. 2 & Suppl. Fig. S2, respectively).

In the negative MN, 412 nodes were generated and grouped as 36 clusters with 88 singletons (Fig. 2). The significant dereplicated sets of the negative MN were cluster A (fatty acids, esters and triacylglycerols), cluster B (flavonoids), clusters C, D and G (unidentified), cluster E (catechin and catechin derivatives), clusters F, H and I (fatty acids alcohols) and cluster J (coumaroyl derivatives) (Fig.3). In contrast, the positive MN encompassed 545 nodes in 42 clusters and 270 discrete nodes, in which cluster A (fatty acids, esters and triacylglycerols), cluster B (triterpenes), cluster C (flavonoids), clusters D, E, F, G, H and I (unidentified) and cluster J (phosphocholine) (Suppl. Fig.S3).

Flavonoids arranged in cluster B (negative MN, Fig.3) and cluster C (positive MN, Suppl. Fig.S3) showed the predominance of green and grey colors signifying that they were more abundant in FR and LR extracts. Quercetin *O*-rhamnoside was the most abundant flavonoid identified, followed by quercetin *O*- hexoside, kaempferol *O*- hexouronide, kaempferol *O*-rhamnoside and quercetin *O*-rutinoside, respectively.

In case of fatty acids alcohols, they were detected in comparable levels in the negative MN (Fig.3 clusters F, H and I) and they were more predominant in FW and FR as donated by the predominance of blue and green colors, respectively.

Cluster A (fatty acids, esters and triacylglycerols) in the negative MN (Fig.3) showed the predominance of green and pink colors signifying that they were more abundant in FR and BR extracts, while the same cluster in the positive MN (Suppl. Fig.S3) showed the predominance of green and blue colors signifying that they were more abundant in FR and FW extracts. In the fatty acids, esters and triacylglycerols clusters, linolenic acid was the most abundant compound identified, followed by octadecadiynoic acid, methyl lineoleate and glyceryl monostearate, respectively.

Triterpenes were detected mainly in the positive MN (Suppl. Fig.S3 cluster B) and they were more predominant in BR and BW as donated by the predominance of pink and yellow colors, respectively. Nor hopanedione was the most abundant terpene identified, followed by oleanadiene.

Catechin and catechin derivatives arranged in cluster E (negative MN, Fig.3) in comparable levels showed the predominance of yellow and grey colors signifying that they were more abundant in BW and LR extracts. Finally, cluster J (coumaroyl derivatives) in the negative MN (Fig.3) showed the predominance of yellow color signifying that they were more abundant in BW extract and they were also in comparable levels.

3.3.1. Identification of simple phenols and flavonoids

For simple phenols, 5 compounds were tentatively identified including, catechol at m/z 109.0288 [M - H]⁻, coumarin at m/z 147.0438 [M + H]⁺ and their derivatives. Pyrocatechuate at m/z 153.0188 [M - H]⁻ and protocatechuic aldehyde at m/z 137.0239 [M - H]- produced a distinguished peak ion at m/z 108 [M - H]⁻of deprotonated catechol. Also, hexosyl-coumarate at m/z 325.0921 [M - H]⁻ produced a distinguished peak ion at m/z 145 [M - H]⁻of deprotonated coumarin. In case of flavonoids, a total of 34 compounds were assigned based on ESI-MS/MS spectra, and further GNPS network aiding in their structural elucidation. Quercetin and kaempferol, were the most abundant flavonols and their glycosides attached to several sugar moieties (e.g., hexose, pentose, rhamnose, acetyl hexose, and rutinoside). For example, the identification of quercetin (peak 17) in the negative mode at m/z 301.0344 [M - H]⁻ with its characteristic product ions at m/z 179 and 151, was detected in further 11 glycoside peaks showing MS2 fragment ion at m/z 301 [M - H]⁻ or 303 [M + H]⁺. Peak 27 at m/z 447.0925 [M-H] ⁻ was annotated as the most abundant flavonoid identified as quercetin *O*-rhamnoside (quercitrin) supported by product ions at m/z 301 [M-H-146] ⁻ for the loss of a deoxyhexoside moiety. Also, the identification of kaempferol (peak 26) in the positive mode at m/z 287.0552 [M+H]⁺ with its characteristic product ions at m/z 153, was detected in further 9 glycoside peaks showing MS2 fragment ion at m/z 285 [M-H]⁻ or 287 [M+H]⁺. The two major flavonoids kaempferol *O*- hexouronide at m/z 463.0875 [M+H]⁺ and kaempferol *O*-rhamnoside at m/z 431.1010 [M-H]⁻ produced a distinguished peak ion at m/z 287 and 285 after the loss of a hexouronide and a deoxyhexoside moieties, respectively. Peak 15 at m/z 609.1451 [M-H]⁻ was annotated as quercetin *O*-rutinoside (rutin) supported by product ion at m/z 301 [M-H-146-162] ⁻ for the loss of a deoxyhexoside and hexose moieties.

3.3.2. Identification of fatty alcohols

A total of 10 fatty alcohols were assigned and detected in comparable levels based on ESI-MS/MS

_____

_____

spectra, and further GNPS network aiding in their structural elucidation. Octadecadienoic acid (linoleic acid) and octadecenoic acid (oleic acid) were detected in the di, tri and tetra hydroxylated form. For example, peak 46 at m/z 313.2375 [M-H]⁻ was annotated as dihydroxy-octadecenoic acid supported by product ion at m/z 201 [M-H-112]⁻ for the loss of a C8H6 group. Hydroxypalmitic acid peak 48 at m/z 271.2271 [M-H]⁻ produced a distinguished peak ion at m/z 253 and 225 after sequential loss of H2O and CO, respectively.

3.3.3.   Identification of triterpenes
A total of 11 pentacyclic triterpenes were assigned based on ESI-MS/MS spectra, and further GNPS network aiding in their structural elucidation. They were pentacyclic triterpenes with a 30-carbon skeleton comprising five, six-membered rings (ursanes, lupanes and hopanes). For example, peak 57 at m/z 427.3575 [M+H]⁺ and peak 62 at m/z 409.3831 [M+H]⁺ were annotated as the most abundant triterpenes identified nor hopanedione and oleanadiene supported by product ion of 100% intensity at m/z 95 [C7H10+H]⁺.

3.3.4.   Identification of fatty acids, esters and triacylglycerols
In total, 27 fatty acids, esters and triacylglycerols were assigned, most of which were unsaturated fatty acids. Linolenic acid peak 69 at m/z 279.2317 [M+H]⁺, methyl lineoleate peak 84 at m/z 295.2627 [M+H]⁺ and glyceryl monostearate peak 87 at m/z 359.3156 [M+H]⁺were the most abundant compounds identified that produced a distinguished peak ion at m/z 109 [C8H12+H]⁺ followed by peak ions at m/z 95, 81 and 67 after sequential loss of CH2 group.

3.4.   Multivariate data analysis

To assess whether the difference in cultivar can affect *P. ellipticum* metabolome, different organs (LR, LW, BR, BW, FR and FW) were analyzed in parallel using UHPLC-HRMS (n = 3) and modelled using unsupervised PCA. Samples segregation was observed along PC1 and PC2 to account for more than 55 % of the total variance (**Fig.** 4). From the PCA scores and loading plots, (Quercetin and Quercetin *O* – hexoside), (Hydroxyoleanolic acid, Norhopanedione and Oleanadiene) and Kaempferol *O*-rhamnoside were the characteristic or discriminant metabolites in leaves, bark and flowers, respectively. To show all the possible links between clusters and to understand our data much better, hierarchical clustering analysis (HCA) was also applied (**Fig.** 5).

Each organ of both cultivars was closely linked. Leaves were linked to bark closer than their link to flowers.

OPLS was further applied for its superiority in classes separation for each organ of both cultivars, obtaining three models with good variance and prediction power (**Fig.** 6-8). By analyzing loading plots and S-loading plots, the characteristic or discriminant metabolites in each organ were identified. Quercetin, quercetin *O*-rhamnoside, quercetin *O*- hexoside and quercetin *O*-hexosyl-acetate were abundant in LR while the LW was further enriched with quercetin *O*-hexouronide, quercetin *O*-rutinoside, quercetin *O*-pentosyl-hexoside and betaine. For bark, lupeone, norhopanedione, oleanadiene and trihydroxyursenoic acid were abundant in BR while the BW was further enriched with catechin, catechin *O*- xyloside, protocatechuic aldehyde and propyloctanoate. Looking for flowers, quercetin, quercetin *O*-rhamnoside, kaempferol *O*-rutinoside and kaempferol *O*-rhamnoside were abundant in FR while the FW was enriched with kaempferol *O*-rhamnoside, epoxyoleic acid, linolenic acid and oxo-octadecadienoic acid.

Depending on PCA and OPLS**,** the discriminant or abundant compounds in *P. ellipticum* cultivars were summarized (**Fig.** 9).

3.5.   In-vitro acetyl and butyryl cholinesterase inhibitory activities
The inhibitory activities of the ethanolic extracts of LR, LW, BR, BW, FR and FW were screened towards AChE and BChE. All extracts exhibited comparable inhibitory activities against AChE with IC₅₀ almost lower than100 µg/mL while they were inactive against BChE with IC₅₀ higher than100 µg/mL (**Table** 2). This work is considered as a step towards investigating the anti-Alzheimer activity of the tested extracts. Although compared to Donepezil (positive standard), the tested extracts didn't show significant anticholinesterase activity, some of the identified metabolites had previously reported anticholinesterase activity[36][37][38]. This drove the author's interest to perform docking studies on these compounds to explore this activity at the molecular level. The results are promising for further investigation for fractionation and isolation of the main active constituents to prove the activity at the pure compounds level.

3.6. Molecular docking study

The binding affinities of the identified compounds from different organs of *P. ellipticum* cultivars

_____

_____

toward the active pocket of co-crystallized donepezil of the AChE target were investigated. This was done to clarify the potential of the examined candidates to act as anti-Alzheimer agents. First, the binding mode of the co-crystallized donepezil of the AChE target receptor clarified that Phe295, Phe389, Asp74, Trp286, and Tyr341 amino acids are crucial for its antagonistic activity. The docked donepezil got a binding score of -8.04 kcal/mol. All the examined compounds of *P. ellipticum* cultivars (major and discriminating metabolites depending on molecular networking and chemometry) showed binding scores in the range of (-4.20 up to -10.50 kcal/mol) with acceptable RMSD values. Notably, pentadecanoyl-docosadienoyl-glycero-phosphoethanolamine, di-linoleoyl-glycero-phosphocholine, kaempferol *O*-rutinoside, and catechin *O*- xyloside were found to be the superior candidates. Their binding scores were recorded to be -10.50, -10.34, -9.14, and -8.69 kcal/mol, which were all better than that of the docked co-crystallized donepezil. This indicates a highly recommended AChE inhibitory potential for the aforementioned members of *P. ellipticum* cultivars. Pentadecanoyl-docosadienoyl-glycero-phosphoethanolamine got stabilized through the formation of two H-pi interactions with Trp286. However, di-linoleoyl-glycero-phosphocholine formed one H-bond with Glu292 and one H-pi bond with Trp286. Besides, kaempferol *O*-rutinoside achieved only a pi-pi interaction with Trp286 of the AChE binding pocket. Finally, catechin *O*- xyloside displayed two H-bonds with Phe295 and Arg296 amino acids (**Table** 3). Accordingly, the previously introduced results proposed the very promising AChE inhibitory potentials of most compounds especially pentadecanoyl-docosadienoyl-glycero-phosphoethanolamine, di-linoleoyl-glycero-phosphocholine, kaempferol *O*-rutinoside, and catechin *O*- xyloside to be tested further either alone or in combination with each other.

4.   Conclusion

Comparable metabolite profiling of *P. ellipticum* cultivars was carried out for the first time *via* UHPLC-MS-based molecular networking in negative and positive ion modes. In total, 89 metabolites belonging to different classes including simple phenols and flavonoids, fatty alcohols, triterpenes, and fatty acids, esters, and triacylglycerols were identified. The significant differences between *P. ellipticum* cultivars and the abundant compounds in each organ were detected by the aid of multivariate data analysis. Also, the inhibitory activities of the studied ethanolic extracts were screened towards AChE and BChE. Although the AChE inhibitory activity of the plant extracts were less compared to the positive control (Donepezil), the results are

promising for further investigation for fractionation and isolation of the main active constituents to prove the activity at the pure compounds level. In addition, our hypothesis was further supported by the molecular docking study for the major identified metabolites that proposed the very promising AChE inhibitory potentials of most compounds to be tested further either alone or in combination with each other.

5.   Authorship contribution statement

6.   Declaration of Competing Interest

The authors declare that they have no known competing financial interests or personal relationships that could have appeared to influence the work reported in this paper.

7.   Funding

8.   Figures and tables

_____
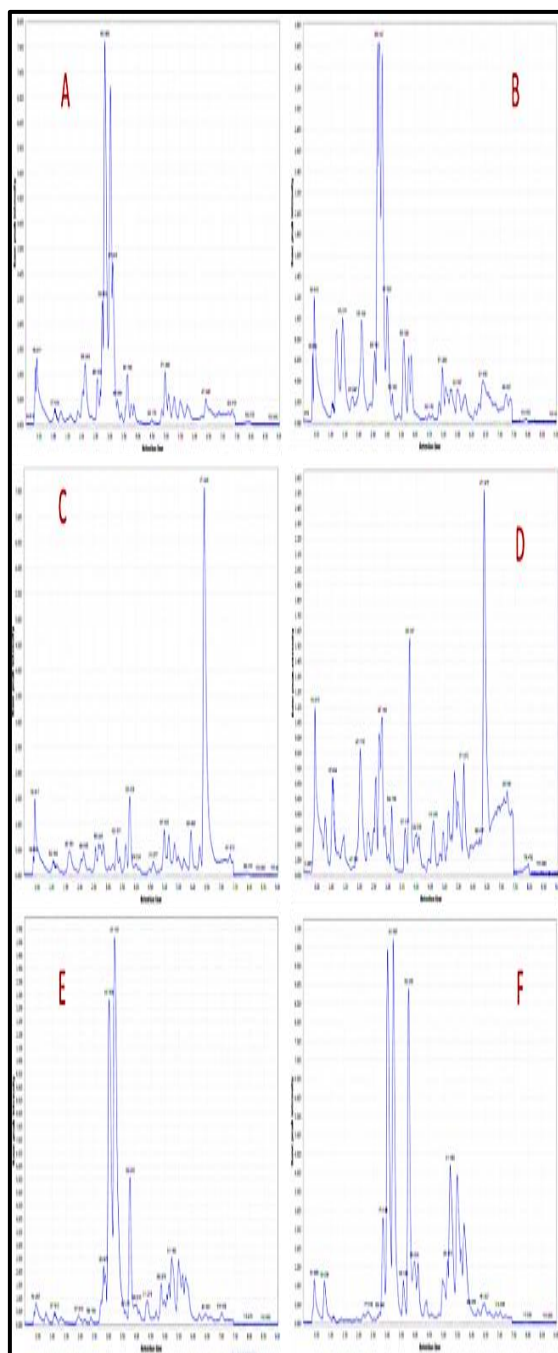
Fig. 1: Base peak chromatograms of LC-MS analysis of *P. ellipticum* leaves; LR (A), LW (B), bark; BR (C) and BW (D) and flowers; FR (E) and FW (F) in negative mode on an UHPLC-ESI-QTOF-MS/MS   instrument

Fig. 2: GNPS molecular network created using MS/MS data in negative mode from ethanolic extracts of *P. ellipticum* Cultivars; LR: Leaves of red, LW: Leaves of white, BR: Bark of red, BW: Bark of white, FR: Flowers of red, FW: Flowers of white. Nodes were labeled with precursor mass (m/z). The network was displayed as pie chart with grey, orange, pink, yellow, green and blue colors representing distribution of the precursor ion intensity in the LR, LW, BR, BW, FR and FW, respectively. The node size represents the sum of precursor ion intensity
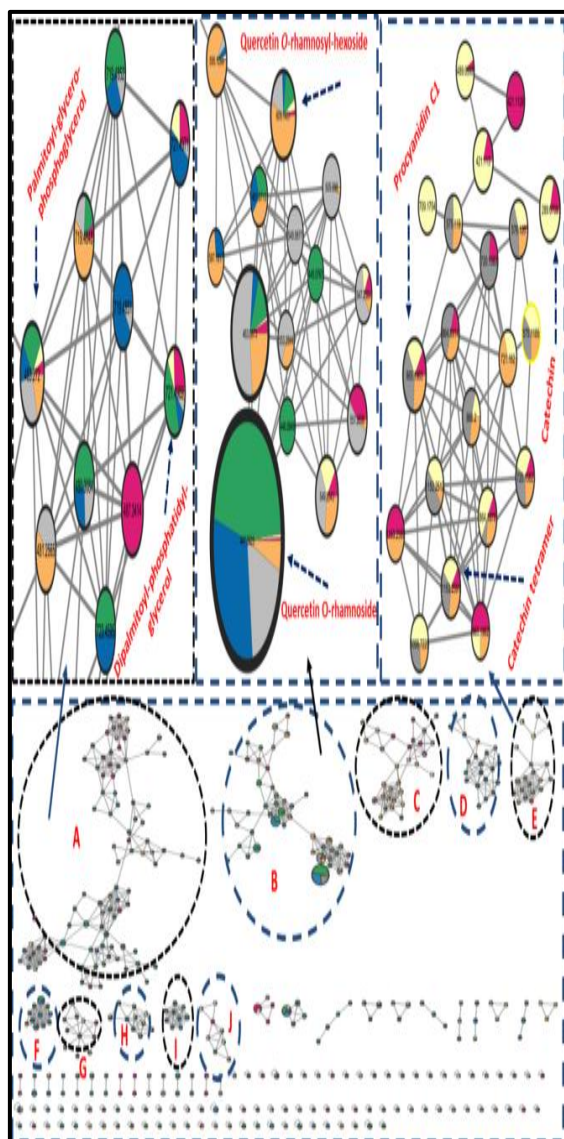
Fig. 3: GNPS molecular network created using MS/MS data in negative mode from ethanolic extracts of *P. ellipticum* Cultivars; LR: Leaves of red, LW: Leaves of white, BR: Bark of red, BW: Bark of white, FR: Flowers of red, FW: Flowers of white with 10 major clusters; cluster A (Fatty acids, esters and triacylglycerols), cluster B (Flavonoids), clusters C, D and G (Unidentified), cluster E (Catechin and catechin derivatives), clusters F, H and I (fatty acids alcohols) and cluster J (Coumaroyl derivatives). Nodes were labeled with precursor mass (*m/z*). The network was displayed as pie chart with grey, orange, pink, yellow, green and blue colors representing distribution of the precursor ion intensity in the LR, LW, BR, BW, FR and FW, respectively. The node size represents the sum of precursor ion intensity.
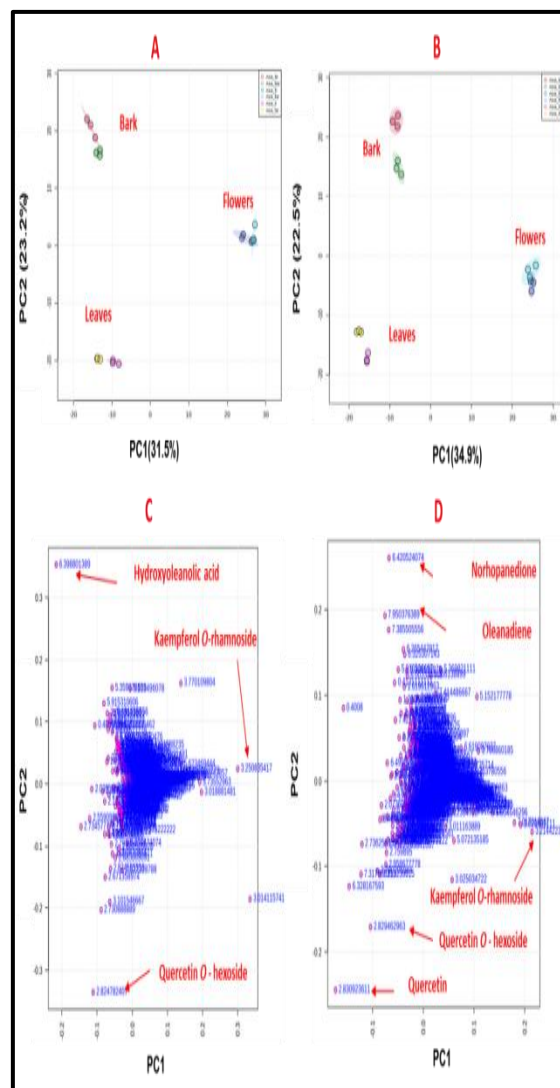

Fig. 4: Principal component analysis (PCA) of modelling *P. ellipticum* leaves, bark and flowers of both cultivars (LR, LW, BR, BW, FR and FW) as analyzed by UHPLC-HRMS (n = 3). (A, C) and (B, D) corresponding to PCA scores and loading plots with comparable total variance in negative and positive modes, respectively. (Quercetin and Quercetin *O* – hexoside), (Hydroxyoleanolic acid, Norhopanedione and Oleanadiene) and Kaempferol *O*-rhamnoside were the more abundant peaks in leaves, bark and flowers, respectively.

_____

Fig. 5: Hierarchical clustering analysis (HCA) of modelling *P. ellipticum* Cultivars; LR: Leaves of red, LW: Leaves of white, BR: Bark of red, BW: Bark of white, FR: Flowers of red, FW: Flowers of white as analyzed by UHPLC-HRMS (n = 3). (A) and (B) corresponding to HCA in negative and positive modes, respectively. Each organ of both cultivars was closely linked. Leaves were linked to bark closer than their link to flowers

Fig. 6: Supervised OPLS-DA scores plot (A and B) and loading S-plots (C and D) as analyzed by HRUHPLC-HRMS (n = 3) for *P. ellipticum* leaves (LR and LW) showed better classification where metabolome clusters are located at distinct positions in negative and positive modes, respectively. Variables at both side end of S. plot corresponded to discriminating metabolites for each organ. Quercetin, quercetin *O*-rhamnoside, quercetin *O*- hexoside and quercetin *O*-hexosyl-acetate were abundant in LR while the LW was further enriched with quercetin *O*-hexouronide, quercetin *O*-rutinoside, quercetin *O*-pentosyl-hexoside and betaine. R2 and Q2 denoted model covered variance and prediction power, respectively
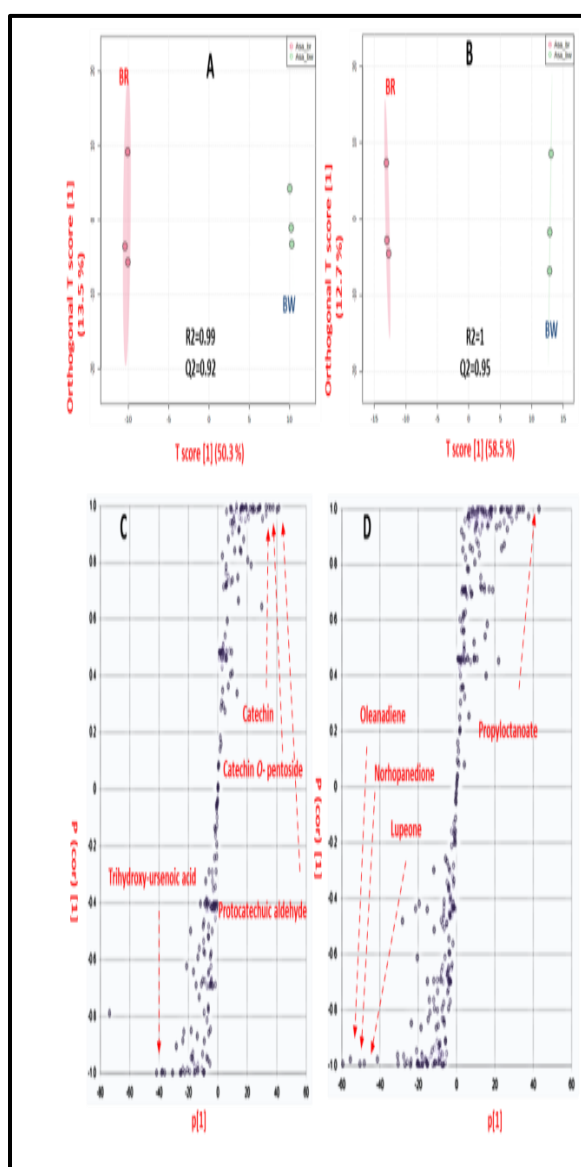
Fig. 7: Supervised OPLS-DA scores plot (A and B) and loading S-plots (C and D) as analyzed by UHPLC-HRMS (n = 3) for *P. ellipticum* bark (BR and BW) showed better classification where metabolome clusters are located at distinct positions in negative and positive modes, respectively. Variables at both side end of S. plot corresponded to discriminating metabolites for each organ. Lupeone, norhopanedione, oleanadiene and trihydroxyursenoic acid were abundant in BR while the BW was further enriched with catechin, catechin *O*- xyloside, protocatechuic aldehyde and propyloctanoate. R2 and Q2 denoted model covered variance and prediction power, respectively.
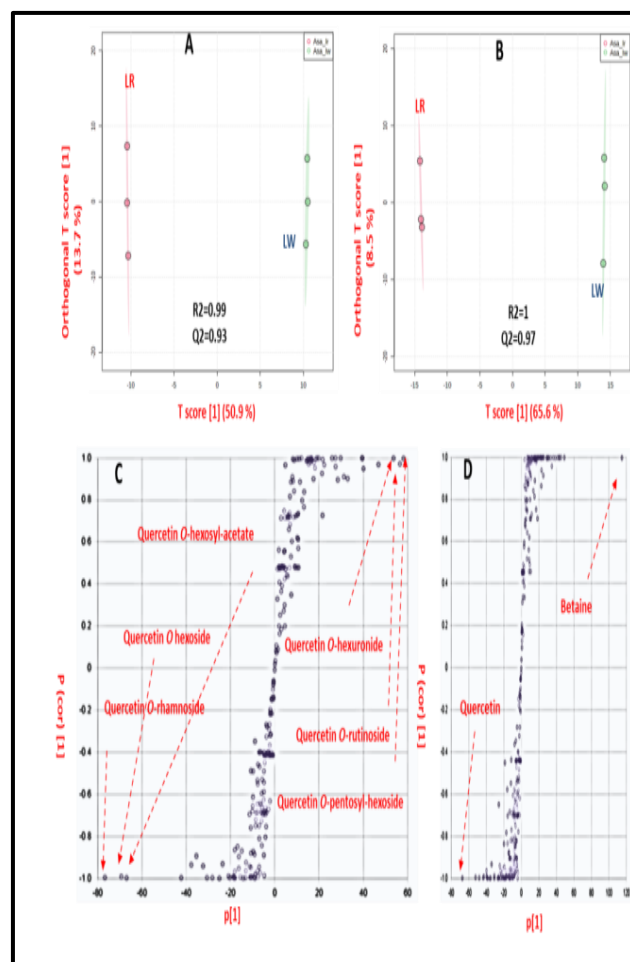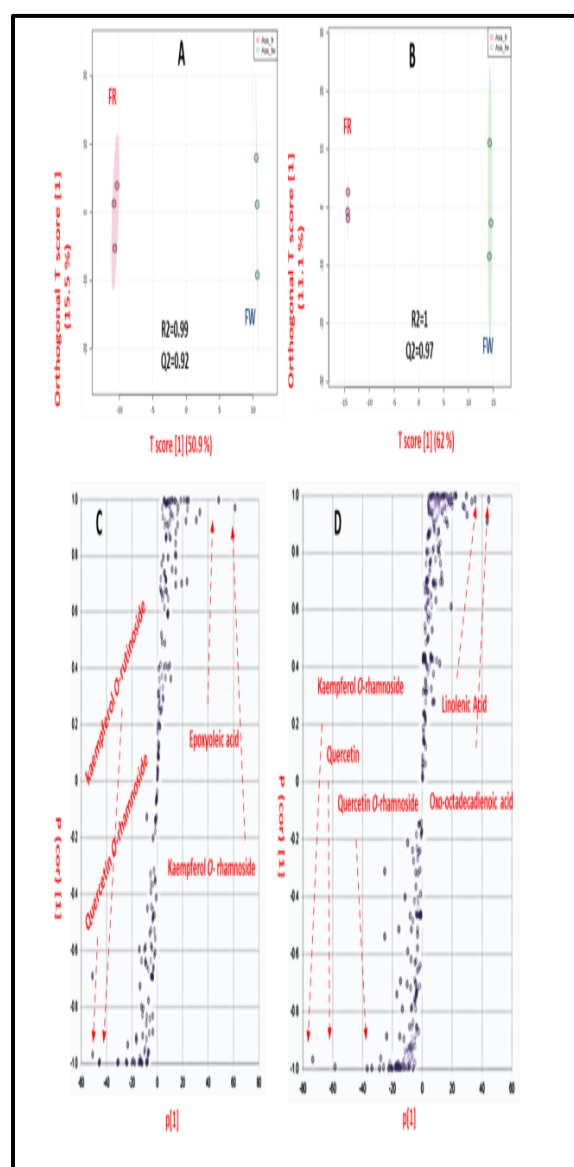
Fig. 8: Supervised OPLS-DA scores plot (A and B) and loading S-plots (C and D) as analyzed by UHPLC-HRMS (n = 3) for *P. ellipticum* flowers (FR and FW) showed better classification where metabolome clusters are located at distinct positions in negative and positive modes, respectively. Variables at both side end of S. plot corresponded to discriminating metabolites for each organ. Quercetin, quercetin *O*-rhamnoside, kaempferol *O*-rutinoside and kaempferol *O*-rhamnoside were abundant in FR while the FW was enriched with kaempferol *O*- rhamnoside, epoxyoleic acid, linolenic acid and oxo-octadecadienoic acid. R2 and Q2 denoted model covered variance and prediction power, respectively.

_____

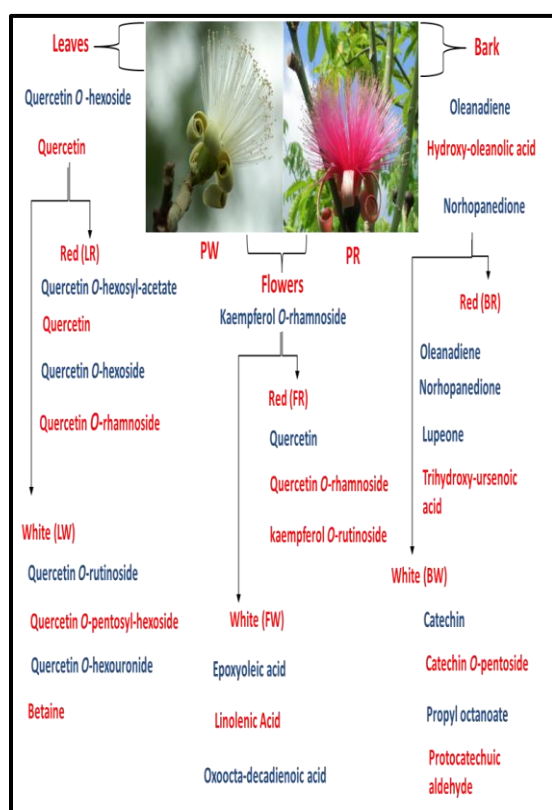**Fig.** 9: Summary of the discriminant or abundant compounds in in the different organs of *P. ellipticum* Cultivars; LR: Leaves of red, LW: Leaves of white, BR: Bark of red, BW: Bark of white, FR: Flowers of red, FW: Flowers of white, depending on PCA and OPLS studies as analyzed by UHPLC-HRMS (n = 3).

Table 1: Identified metabolites in the different organs of *P. ellipticum* Cultivars; leaves (LR and LW), bark (BR and BW) and flowers (FR and FW).

Comp. number	Rt time (min)	[M - H]⁻	[M + H]⁺	MS2 (m/z)	Adduct Mol. formula	Proposed structure	Ref.	LR	LW	BR	BW	FR	FW	Error PPM
Simple phenols and flavonoids														
1.	0.78	153.0188		109, 108, 81	$C_7H_5O_4^-$	Pyrocatechuate	[2]	+	+	+	+	+	+	-5.3
2.	0.78	109.0288		108, 91, 81, 53	$C_6H_5O_2^-$	Catechol	[39]	+	+	+	+	+	+	-6.1
3.	1.05	137.0239		136, 108, 92, 81, 53	$C_7H_5O_3^-$	Protocatechuic aldehyde	[39]	+	+	+	+	-	-	-6.8
4.	1.1		147.0438	119, 91, 65	$C_9H_7O_2^+$	Coumarin	[40]	+	+	+	+	+	+	-4.7
5.	1.33	325.0921		145, 119, 59	$C_{15}H_{17}O_8^-$	Hexosyl -coumarate	[41]	+	+	+	-	+	+	-7.9
6.	2.03	421.1130		289, 245	$C_{20}H_{21}O_{10}^-$	Catechin *O*- pentoside	[2]	+	+	+	+	+	+	-5.1
7.	2.05	289.0709	291.0863	147, 139, 123	$C_{15}H_{15}O_6^+$	Catechin / Epicatechin	[2]	+	+	+	+	-	-	-2.6
8.	2.19	593.1501	595.1657	383, 353	$C_{27}H_{28}O_{15}^-$	Apigenin di-C-hexosyl	[2]	-	+	-	+	-	+	-3.1
9.	2.21	865.1962	867.2122	407, 289, 125	$C_{45}H_{37}O_{18}^-$	Procyanidin C1	[2]	+	+	+	+	-	-	-1.0
10.	2.44	757.1815		595, 300	$C_{32}H_{36}O_{21}^-$	Quercetin di-*O*- hexoside - pentoside	[2]	-	+	-	-	-	-	-1.1
11.	2.52	625.1396		301, 300	$C_{27}H_{28}O_{17}^-$	Quercetin di-*O*- hexoside	[2]	+	+	-	-	-	-	-3.7
12.	2.67	595.1299	597.1454	300	$C_{26}H_{26}O_{16}^-$	Quercetin *O*-pentosyl- hexoside	[2]	+	+	+	+	-	+	-4.5
13.	2.69	1153.2591	1155.2745	407, 289, 125	$C_{60}H_{49}O_{24}^-$	Catechin tetramer	[41]	+	+	+	+	-	-	-6.9
14.	2.71	785.2135		314, 299	$C_{34}H_{40}O_{21}^-$	Isorhamnetin di-*O*- rutinoside-hexoside	[42]	-	-	-	-	+	-	-3.8
15.	2.73	609.1451	611.1609	301, 300	$C_{27}H_{28}O_{16}^-$	Quercetin *O*- rutinoside	[2]	+	+	+	+	+	+	-3.1
16.	2.82	463.0873	465.1033	301, 300, 271	$C_{21}H_{18}O_{12}^-$	Quercetin *O*- hexoside	[2]	+	+	+	+	+	+	-4.6
17.	2.83	301.0344	303.0501	257, 229, 153	$C_{15}H_{10}O_7^+$	Quercetin	[2]	+	+	+	+	+	+	-4.3
18.	2.83	477.0663	479.0827	301, 179, 151	$C_{21}H_{16}O_{13}^-$	Quercetin *O*-hexouronide	[41]	+	+	+	-	+	+	-3.6
19.	2.83	577.1341		285, 284, 255	$C_{30}H_{24}O_{12}^-$	Kaempferol *O-p*-coumaroyl-rhamnoside	[43]	-	+	+	-	-	-	-3.4
20.	2.86	579.1348		285, 284, 255	$C_{26}H_{26}O_{15}^-$	Rustoside	[42]	+	+	-	-	-	+	-3.5
21.	2.88		449.1083	447, 285	$C_{21}H_{20}O_{11}^+$	Kaempferol *O*- hexoside	[2]	-	+	-	-	-	-	-6.5
22.	2.89	593.1497	595.1662	285, 284, 255	$C_{27}H_{28}O_{15}^-$	kaempferol *O*-rutinoside	[2]	+	+	+	+	+	+	-3.3
23.	2.92	623.1603	625.1769	315, 314, 300	$C_{28}H_{30}O_{16}^-$	Isorhamnetin *O*-rutinoside	[2]	+	+	+	-	-	-	-4.1
24.	2.96	505.0980		301, 300, 271, 255	$C_{23}H_{20}O_{13}^-$	Quercetin *O*-hexosyl-acetate	[42]	+	+	-	-	-	-	1
25.	2.96	549.0877	551.1034	301, 300, 271, 255	$C_{24}H_{20}O_{15}^-$	Quercetin *O*-malonyl hexoside	[44]	+	-	-	-	-	-	-5.1
26.	2.99		287.0552	165, 153	$C_{15}H_{10}O_6^+$	Kaempferol	[2]	+	+	-	-	+	+	-1.6
27.	3.01	447.0925	449.1083	301, 271, 255, 151	$C_{21}H_{18}O_{11}^-$	Quercetin *O*-rhamnoside	[2]	+	+	+	+	+	+	-4.5
28.	3.02		463.0875	287, 153	$C_{21}H_{19}O_{12}^+$	Kaempferol *O*- hexouronide	[41]	-	+	-	-	+	+	-0.7
29.	3.13	417.0816		285, 284, 255, 227	$C_{20}H_{17}O_{10}^-$	kaempferol *O*-pentoside	[42]	-	-	-	-	+	+	-3.1
30.	3.16	461.1070		299, 284	$C_{22}H_{21}O_{11}^-$	Hispidulin *O*-hexoside	[45]	+	+	+	-	+	+	-2.6
31.	3.17		463.1232	317, 301	$C_{22}H_{23}O_{11}^+$	Rhamnetin *O*-rhamnoside	[2]	+	+	+	-	-	-	-.8
32.	3.21	431.1010	433.1134	285, 284, 255, 227	$C_{21}H_{19}O_{10}^-$	kaempferol *O*-rhamnoside	[2]	+	-	-	-	+	+	-2.0

Comp. number	Rt time (min)	[M - H]⁻	[M + H]⁺	MS2 (m/z)	Adduct Mol. formula	Proposed structure	Ref.	LR	LW	BR	BW	FR	FW	Error PPM
33.	3.21	563.1396		285, 284, 255, 227	$C_{26}H_{27}O_{14}^-$	Kaempferol *O*-rhamnosyl-pentoside	[42]	-	+	-	-	+	+	-2.2
34.	3.23	491.0822	493.0992	315, 300	$C_{22}H_{19}O_{13}^-$	Quercetin di-*O*-methyl ether-hexuronide	[41]	+	-	-	-	+	+	-4.3
35.	3.27		479.1181	317	$C_{22}H_{23}O_{12}^+$	Isorhamnetin *O*- hexoside	[42]	+	-	+	-	-	-	0.0
36.	3.41	609.1246		463, 301, 300, 255	$C_{30}H_{25}O_{14}^-$	Quercetin di-*O*-*p*-coumaroyl-hexoside	[43]	+	+	-	-	+	+	-3.6
37.	3.56	623.1392		315, 299, 271, 255	$C_{31}H_{27}O_{14}^-$	Isorhamnetin di-*O*- *p*-coumaroyl- hexoside	[43]	-	-	-	-	+	+	-2.1
38.	3.58	593.1300	595.1454	287, 147, 119	$C_{30}H_{27}O_{13}^+$	kaempferol di-*O*- *p*-coumaroyl-hexoside	[43]	+	+	-	-	+	+	-3.1
39.	3.63		317.0656	302, 179, 167	$C_{16}H_{13}O_7^+$	Rhamnetin	[2]	+	-	+	-	-	+	-2.7
Fatty amides and alcohols														
40.	0.4		104.1068	60, 58	$C_5H_{14}NO^+$	Choline	[46]	+	+	+	+	+	+	2.1
41.	0.42		118.0860	59, 58	$C_5H_{12}NO_2^+$	Betaine	[46]	+	+	+	+	+	+	0.8
42.	2.94	343.2118		229, 211, 171, 83	$C_{18}H_{31}O_6^-$	Tetrahydroxy-octadecadienoic acid	[47]	-	-	-	-	+	+	-8.0
43.	3.60	327.2169		229, 211, 171, 99	$C_{18}H_{31}O_5^-$	Trihydroxy-octadecadienoic acid	[2]	+	+	+	+	+	+	-6.2
44.	3.77	329.2325		229, 211, 171, 139, 99	$C_{18}H_{33}O_5^-$	Trihydroxy-octadecenoic acid	[47]	+	+	+	+	+	+	-0.2
45.	4.44	309.2066		199, 183, 181, 155	$C_{18}H_{29}O_4^-$	Hydroperoxy-octadecatrienoic acid	[48]	+	+	+	+	+	+	-1.6
46.	4.59	313.2375		295, 201, 183, 129, 99	$C_{18}H_{33}O_4^-$	Dihydroxy-octadecenoic acid	[49]	+	+	+	+	+	+	5.5
47.	4.77	311.2220		295, 199, 183, 129	$C_{18}H_{31}O_4^-$	Dihydroxy-octadecadienoic acid	[49]	+	-	+	+	+	+	-1.7
48.	5.68	271.2271		253, 225, 223	$C_{16}H_{31}O_3^-$	Hydroxypalmitic acid	[47]	+	+	+	+	+	+	-3.1
49.	6.50	327.2894		281	$C_{20}H_{39}O_3^-$	Hydroxyeicosanoic acid	[47]	+	+	+	+	+	+	-3.9
50.	7.06	369.3365		323	$C_{23}H_{45}O_3^-$	Hydroxytricosanoic acid	[50]	+	+	+	+	+	+	-2.8
51.	7.22	383.3526		337	$C_{24}H_{47}O_3^-$	Hydroxytetracosanoic acid	[50]	+	+	+	+	+	+	-1.5
Triterpens														
52.	4.99	487.3414		255, 153	$C_{30}H_{47}O_5^-$	Trihydroxy-ursenoic acid	[47]	-	-	+	-	-	-	-3.7
53.	5.92	439.3569 (M+H-H2O)		203, 137, 123, 95, 81	$C_{30}H_{47}O_2$	Betulinic acid	[51]	+	+	+	+	-	+	0.0
54.	6.27		441.3728	287, 135, 121, 95, 81	$C_{30}H_{49}O_2^+$	Ursolic aldehyde	[47]	+	+	+	+	-	+	-3.0
55.	6.38	469.3674		427, 409, 393	$C_{31}H_{49}O_3^-$	Acetoxy-nor lupenone	[2]	+	-	-	-	-	-	1.7
56.	6.40	471.3474		427, 409, 393	$C_{30}H_{47}O_4^-$	Hydroxy-oleanolic acid	[2]	+	+	+	+	-	-	-1.2
57.	6.42		427.3575	281, 147, 121, 95, 81	$C_{29}H_{47}O_2^+$	Nor hopanedione	[2]	+	+	+	+	+	+	-3.3
58.	6.57		425.3769	135, 109, 95, 81, 69	$C_{30}H_{49}O^+$	Lupeone	[2]	+	+	+	+	+	+	-7.1
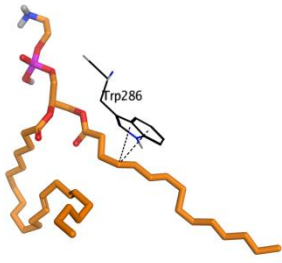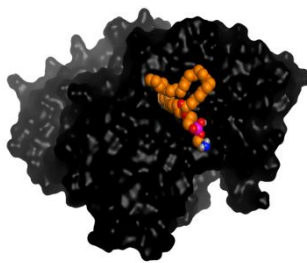
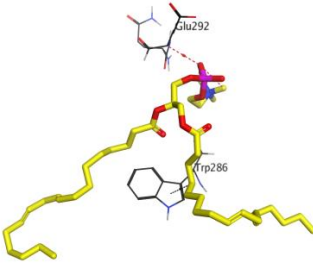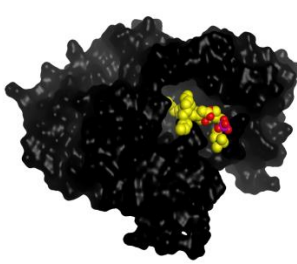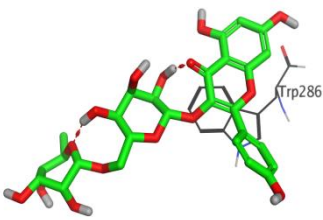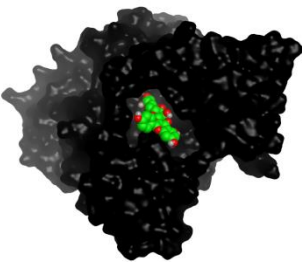| Comp. number	Rt time (min)	[M - H]⁻	[M + H]⁺	MS2 (m/z)	Adduct Mol. formula	Proposed structure	Ref.	LR	LW	BR	BW	FR	FW	Error PPM
59.	6.63		423.3619	187, 137, 109, 81, 69	$C_{30}H_{47}O^+$	Lupadienone	[2]	+	+	+	+	-	+	-3.5
60.	6.67		413.3765	299, 159, 121, 81, 69	$C_{29}H_{49}O^+$	Nor lupeol	[2]	+	+	+	+	+	+	-5.3
61.	7.32		443.3883	135, 109, 95, 81, 69	$C_{30}H_{51}O_2^+$	Hydroxy-beta-amyrin	[2]	+	+	+	+	-	-	-2.0
62.	7.42		409.3831	137, 109, 95, 81, 69	$C_{30}H_{49}^+$	Oleanadiene	[52]	+	+	+	+	-	-	-0.8
Fatty acids, esters and triacylglycerols														
63.	4.38		538.3502	184, 104, 86, 60	$C_{26}H_{53}NO_8P^+$	Hydroxyoleoyl-glycero-phosphocholine	[53]	-	-	-	-	+	+	-2.4
64.	4.79		518.3239	184, 124, 104, 86, 60	$C_{26}H_{49}NO_7P^+$	Linolenoyl-glycero-phosphocholine	[53]	-	+	-	+	+	+	-3.1
65.	4.82		337.2690	123, 109, 95, 81, 67	$C_{21}H_{37}O_3^+$	Glycidyl-linoleate	[2]	-	-	-	+	+	+	-5.4
66.	4.89		353.2683	125, 95, 81, 67, 57	$C_{21}H_{38}O_4^+$	Linolenoyl-glycerol	[2]	+	+	+	+	+	+	-4.0
67.	4.98		520.3400	184, 125, 104, 86, 60	$C_{26}H_{51}NO_7P^+$	Linoleoyl-glycero-phosphocholine	[53]	+	+	+	+	+	+	0.0
68.	5.07		496.3404	184, 125, 104, 86	$C_{24}H_{51}NO_7P^+$	Palmitoyl-glycero-phosphocholine	[53]	+	+	+	+	+	+	-0.0
69.	5.15		279.2317	109, 95, 81, 67	$C_{18}H_{31}O_2^+$	Linolenic acid	[2]	+	+	+	+	+	+	-4.6
70.	5.16	295.2290		184, 183	$C_{18}H_{31}O_3^-$	Oxo-octadecenoic acid	[2]	+	+	+	+	+	+	1.8
71.	5.21		522.3560	184, 125, 104, 86, 60	$C_{26}H_{53}NO_7P^+$	Octadecenoyl-glycero-phosphocholine	[53]	+	+	+	+	+	+	-2.2
72.	5.27	297.2426		279, 199, 183, 171	$C_{18}H_{33}O_3^-$	Epoxyoleic acid	[54]	-	-	+	+	+	+	-4.7
73.	5.29		263.2367	95, 81, 67	$C_{18}H_{31}O^+$	Linolenyl aldehyde	[2]	-	-	+	+	+	+	-6.5
74.	5.35	433.2352		153, 79	$C_{21}H_{38}O_7P^-$	Linoleoyl-glycero-phosphate	[49]	-	+	+	+	+	+	-0.9
75.	5.35	599.3191		283, 241, 153, 79	$C_{27}H_{52}O_{12}P^-$	Stearoyl-glycero-phosphoinositol	[49]	+	+	+	+	+	+	-4.1
76.	5.37	293.2113	295.2269	107, 95, 81, 69, 55	$C_{18}H_{31}O_3^+$	Oxo-octadecadienoic acid	[49]	+	+	+	+	+	+	-4.5
77.	5.37		277.2160	107, 93, 81, 67, 55	$C_{18}H_{29}O_2^+$	Octadecadiynoic acid	[2]	+	+	+	+	+	+	-4.4
78.	5.50		524.3715	184, 125, 104, 86	$C_{26}H_{55}NO_7P^+$	Stearoyl-glycero-phosphocholine	[53]	+	+	+	+	+	+	-6.0
79.	5.51		297.2422	107, 97, 81, 67, 55	$C_{18}H_{33}O_3^+$	Epoxy-octadecenoic acid	[54]	-	-	+	+	+	+	-3.4
80.	5.69	435.2505		267, 167, 153, 79	$C_{21}H_{40}O_7P^-$	Oleoyl-lysophosphatidic acid	[55]	-	-	+	+	+	+	-5.4
81.	5.75		355.2841	109, 95, 81, 67, 57	$C_{21}H_{39}O_4^+$	Linoleoyl-glycerol	[2]	+	-	+	+	+	+	-4.7
82.	5.87		313.2738	95, 85, 71, 57	$C_{19}H_{37}O_3^+$	Methyl-epoxystearate	[54]	+	+	+	+	+	+	-2.9
83.	5.87		331.2842	95, 85, 71, 57	$C_{19}H_{39}O_4^+$	Glyceryl palmitate	[2]	+	+	+	+	+	+	0.1
84.	5.87		295.2627	109, 95, 81, 69, 55	$C_{19}H_{35}O_2^+$	Methyl lineoleate	[2]	-	-	-	-	+	+	-5.8
85.	6.01		309.2427	107, 93, 81, 79, 55	$C_{19}H_{33}O_3^+$	Oxo-octadecadienoic acid methyl ester	[2]	-	-	-	-	+	+	-3.6
86.	6.15		311.2584	109, 95, 81, 67, 57	$C_{19}H_{35}O_3^+$	Methyl-epoxyoleate	[54]	-	-	-	-	+	+	-3.5
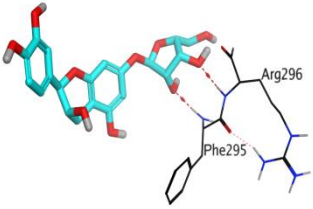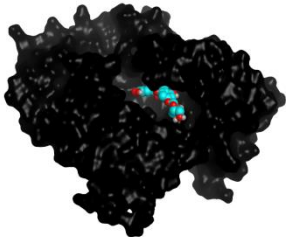
Comp. number	Rt time (min)	[M - H]$^-$	[M + H]$^+$	MS2 (m/z)	Adduct Mol. formula	Proposed structure	Ref.	LR	LW	BR	BW	FR	FW	Error PPM
87.	6.29		359.3156	109, 95, 71, 57	$C_{21}H_{43}O_4^+$	Glyceryl monostearate	[54]	+	+	+	+	+	+	-4.4
88.	6.30	756.5608		532, 278, 101, 89, 71, 59	$C_{42}H_{80}NO_8P^-$	Pentadecanoyl-docosadienoyl-glycero-phosphoethanolamine	[56]	-	-	-	-	+	+	-4,8
89.	7.94		782.5689	184, 125, 86	$C_{44}H_{80}NO_8P^+$	Dilinoleoyl-glycero-phosphocholine	[53]	-	-	+	+	+	+	-3,6

Table 2: In-vitro inhibitory activities of the ethanolic extracts of different organs of P. ellipticum Cultivars; leaves (LR and LW), bark (BR and BW) and flowers (FR and FW), towards AChE and BChE

Samples	% inhibition against AChE		% inhibition against BChE	
	at 10 µg/mL	at 100 µg/mL	at 10 µg/mL	at 100 µg/mL
LR	26.43 ± 3.55	60.22 ± 5.81	Undetected	25.79 ± 2.53
LW	24.14 ± 1.87	58.43 ± 3.98	Undetected	26.59 ± 3.38
BR	24.00 ± 3.11	60.53 ± 2.75	Undetected	24.45 ± 1.05
BW	30.14 ± 0.99	57.01 ± 3.23	Undetected	28.22 ± 2.58
FR	26.93 ± 2.63	51.03 ± 2.41	Undetected	Undetected
FW	Undetected	55.98 ± 3.09	Undetected	27.96 ± 1.98
Standard Donepezil	66.54 ± 1.22 at 2.08 ng/mL		61.15 ± 1.08 at 0.416 µg/mL	

Table 3: 3D interactions and positioning within the donepezil binding pocket of AChE (PDB ID: 4EY7) for 1-pentadecanoyl-2-docosadienoyl-glycero-3-phosphoethanolamine, 1,2-dilinoleoyl-sn-glycero-3-phosphocholine, kaempferol *O*-rutinoside, and catechin *O*- xyloside.

Comp.	3D interactions	3D positioning
1-Pentadecanoyl-2-docosadienoyl-glycero-3-phosphoethanolamine		
1,2-Dilinoleoyl-sn-glycero-3-phosphocholine		
Kaempferol *O*-rutinoside		

_____

Comp.	3D interactions	3D positioning
Catechin *O*- xyloside		

9. References

[1]   J.K. Das, G.; Shin, H.-S.; Ningthoujam, S.S.; Talukdar, A.D.; Upadhyaya, H.; Tundis, R.; Das, S.K.; Patra, Systematics, Phytochemistry, Biological Activities and Health Promoting Effects of the Plants from the Subfamily Bombacoideae (Family Malvaceae), Plants. 10 (2021) 1–38.

[2]   J. Refaat, S.Y. Desoky, M.A. Ramadan, M.S. Kamel, Bombacaceae: A phytochemical review, 2013. https://doi.org/10.3109/13880209.2012.698286.

[3]   A. Ankli, M. Heinrich, P. Bork, L. Wolfram, P. Bauerfeind, R. Brun, C. Schmid, C. Weiss, R. Bruggisser, J. Gertsch, M. Wasescha, O. Sticher, Yucatec Mayan medicinal plants: Evaluation based on indigenous uses, J. Ethnopharmacol. 79 (2002) 43–52. https://doi.org/10.1016/S0378-8741(01)00355-5.

[4]   C.C. Walker, A survey of succulents of the mallow family (Malvaceae), CactusWorld. 39 (2) (2021) 135–148.

[5]   R.C. Díaz, G. Espinosa, C.A. Ilizaliturri, D. González, V.G. Cilia, Antioxidant Activity Assessment of Plants Used in Huastec Traditional Medicine, Mexico, 2015.

[6]   A. Chávez-Piña, A. Sandoval1, A.M.F. , Jesús Arrieta1 , Benito Reyes, and A. Navarrete, Gastroprotective effect of β-LupeoL: roLe of prostaGLandins, suLfhydryLs and nitric oxide, Rev. Latinoamer. 37/2 (2009) 133–143. https://www.researchgate.net/publication/228818031.

[7]   Ahmed S. Mohamed, Omnia Y. Abd El Dayem, Ali M. El Shamy, F.S.E.S. and R.A.E.G. Comparative antisickling and antioxidant activities of Pseudobombax ellipticum cultivars in relation to their metabolite profiling using LC/MS, RSC Adv. 13 (2023) 21327–21335. https://doi.org/10.1039/d3ra03312k.

[8]   Santos ECG, Donnici CL, Camargos ERS, Araújo-Silva G, Xavier-Junior FH, Farias LM, Interaction of Pseudobombax marginatum Robyns Stem Bark Extract on the Cell Surface of Bacillus cereus and Staphylococcus aureus, J Bacteriol Mycol. 5 (2018) 1063.

[9]   Zeinab T. Abdel Shakour, Radwa H. El-Akad, Abdelsamed I. Elshamy , Abd El-Nasser G. El Gendy, Ludger A., M.A.F. Wessjohann, Dissection of Moringa oleifera leaf metabolome in context of its different extracts, origin and in relationship to its biological effects as analysed using molecular networking and chemometrics, Food Chem. 399 (2023).

[10]   S. Gauthier, P. Rosa-Neto, J. Morais, C. Webster, World Alzheimer Report 2021: Journey through the diagnosis of dementia, Alzheimer's Dis. Int. (2021). https://www.alzint.org/resource/world-alzheimer-report-2021/.

[11]   A.A. Hamed, A.A.; El-Shiekh, R.A.; Mohamed, O.G.; Aboutabl, E.A.; Fathy, F.I.; Fawzy, G.A.; Al-Taweel, A.M.; Elsayed, T.R.; Tripathi, A.; Al-Karmalawy, Cholinesterase Inhibitors from an Endophytic Fungus Aspergillus niveus Fv-er401: Metabolomics, Isolation and Molecular Docking, Molecules. 28 (2023). https://pubmed.ncbi.nlm.nih.gov/31335056/.

[12]   S.M. Soheili M, Karimian M, Hamidi GhA, Alzheimer's disease treatment: The share of herbal medicines, Iran J Basic Med Sci. 24 (2021) 123–135. https://doi.org/doi: 10.22038/IJBMS.2020.50536.11512 Introduction.

[13]   M.B. Colovic, D.Z. Krstic, T.D. Lazarevic-Pasti, A.M. Bondzic, V.M. Vasic, Acetylcholinesterase Inhibitors: Pharmacology and Toxicology, Curr. Neuropharmacol. 11 (2013) 315–335. https://doi.org/10.2174/1570159x11311030006.

[14]   D.F. Maulana Yusuf Alkandahri, Recky Patala, Mutiarika Indah Pratiwi, Lilis Setianingsih Agustina, Farhamzah, Anggun Hari Kusumawati, Himyatul Hidayah, Surya Amal, Pharmacological Studies of Durio Zibethinus: A Medicinal Plant Review, Ann. R.S.C.B. 25 (2021) 640–646.

_____

[15]   B. Sultana, F. Anwar, M. Ashraf, Effect of extraction solvent/technique on the antioxidant activity of selected medicinal plant extracts, Molecules. 14 (2009) 2167–2180. https://doi.org/10.3390/molecules14062167.

[16]   P.S. Vankar, J. Srivastava, Evaluation of Anthocyanin Content in Red and Blue Flowers, Int. J. Food Eng. 6 (2010). https://doi.org/10.2202/1556-3758.1907.

[17]   Junaid R Shaikh and MK Patil, Qualitative tests for preliminary phytochemical screening: An overview, International Journal of Chemical Studies 2020; 8(2): 603-608.

[18]   E. Attard, A rapid microtitre plate Folin-Ciocalteu method for the assessment of polyphenols, Cent. Eur. J. Biol. 8 (2013) 48–53. https://doi.org/10.2478/s11535-012-0107-3.

[19]   M. Kiranmai, C.B.M. Kumar, M. Ibrahim, Comparison of total flavanoid content of Azadirachta indica root bark extracts prepared by different methods of extraction, RJPBCS. 2 (2011) 254–261.

[20]   Asmaa M. Otify, Osama G. Mohamed, Yasser A. El-Amier, Fatema R. Saber, Ashootosh Tripathi, I.Y.Y. Bioherbicidal Activity and Metabolic Profiling of Allelopathic Metabolites of Three Cassia species using UPLC-qTOF-MS/MS and Molecular Networking, Metabolomics. 19 (2023).

[21]   Mahmoud A.M. Arafat, Mohammed N.A. Khalil, Osama G. Mohamed, Omnia A.M. Abd El-Ghafar, Ashootosh Tripathi , Engy A. Mahrous, Essam M. Abd El-kader, S.E.-H. Vetiver aerial parts and roots ameliorate rheumatoid arthritis in complete Freund's adjuvant rat model, a phytochemical profiling and mechanistic study, J. Ethnopharmacol. 317 (2023).

[22]   T. Pluskal, S. Castillo, A. Villar-Briones, M. Orešič, MZmine 2: Modular framework for processing, visualizing, and analyzing mass spectrometry-based molecular profile data, BMC Bioinformatics. 11 (2010). https://doi.org/10.1186/1471-2105-11-395.

[23]   Louis-Félix Nothias, *et al.*, Feature-Based Molecular Networking in the GNPS Analysis Environment, Nat Methods. 17 (2020) 905–908. https://doi.org/10.1038/s41592-020-0933-6.

[24]   P. Shannon, A. Markiel, O. Ozier, N.S. Baliga, J.T. Wang, D. Ramage, N. Amin, B. Schwikowski, T. Ideker, Cytoscape: A software Environment for integrated models of biomolecular interaction networks, Genome Res. 13 (2003) 2498–2504. https://doi.org/10.1101/gr.1239303.

[25]   Sherif M. Afifi, Amira El-Mahis, Andreas G. Heiss, M.A.F. Gas Chromatography−Mass Spectrometry-Based Classification of 12 Fennel (Foeniculum vulgare Miller) Varieties Based on Their Aroma Profiles and Estragole Levels as Analyzed Using Chemometric Tools, ACS Omega. 6 (2021) 5775−5785.

[26]   M.A. Farag, I.M.K. , Dalia M. Rasheed, Volatiles and primary metabolites profiling in two Hibiscus sabdariffa (roselle) cultivars via headspace SPME-GC-MS and chemometrics, Food Res. Int. 78 (2015) 327–335.

[27]   Y. kia, H. Osman, R.S. Kumar, A. Basiri, V. Murugaiyah, Ionic liquid mediated synthesis of mono- and bis-spirooxindole-hexahydropyrrolidines as cholinesterase inhibitors and their molecular docking studies, Bioorg. Med. Chem. 22 (2014) 1318–1328. https://doi.org/https://doi.org/10.1016/j.bmc.2014.01.002.

[28]   G.L. Ellman, K.D. Courtney, V. Andres, R.M. Featherstone, A new and rapid colorimetric determination of acetylcholinesterase activity, Biochem. Pharmacol. 7 (1961) 88–95. https://doi.org/https://doi.org/10.1016/0006-2952(61)90145-9.

[29]   R. Huey, G.M. Morris, S. Forli, Using AutoDock 4 and AutoDock Vina with AutoDockTools: A Tutorial, Scripps Res. Inst. Mol. (2012) 32.

[30]   ERIC F. PETTERSEN, THOMAS D. GODDARD, CONRAD C. HUANG, GREGORY S. COUCH, DANIEL M. GREENBLATT, ELAINE C. MENG, UCSF Chimera, T.E.F., A Visualization System for Exploratory Research and Analysis, J Comput Chem. 25 (2004) 1605–1612.

[31]   Faten Farouk, Ayman Abo Elmaaty, Ahmed Elkamhawy, Haytham O. Tawfik, Radwan Alnajjar, Mohammed A. S. Abourehab, Mohamed A. Saleh, W.M.E.& A.A.A. Investigating the potential anticancer activities of antibiotics as topoisomerase II inhibitors and DNA intercalators: in vitro, molecular docking, molecular dynamics, and SAR studies, J. Enzyme Inhib. Med. Chem. 38 (2023).

[32]   Ahmed A. Al-Karmalawy,* Mohamed S. Nafie, Moataz A. Shaldam, Ayman Abo Elmaaty, Samar A. Antar, Ligand-Based Design on the Dog-Bone-Shaped BIBR1532 Pharmacophoric Features and Synthesis of Novel Analogues as Promising Telomerase Inhibitors with In Vitro and In Vivo Evaluations, J. Med. Chem. 66 (2023) 777−792.

[33]   Samia M. Al-Muntaser, Ahmed A. Al-Karmalawy, Abeer M. El-Naggar, Ali Khalil Ali, N.E.A.A.E.-S. a and E.M.A.Novel 4-thiophenyl-pyrazole, pyridine, and pyrimidine derivatives as potential antitumor candidates targeting both EGFR and VEGFR-2; design, synthesis, biological evaluations, and in silico studies, RSC Adv., ,12184. 13 (2023) 12184–12203.

[34]   Mohamed M. Khalifaa, Ahmed A. Al-Karmalawyb, Eslam B. Elkaeedc, I.H.E. and H.A.M., Topo II inhibition and DNA intercalation by new phthalazine-based derivatives as potent anticancer agents: design, synthesis, anti-proliferative, docking,

_____

and in vivo studies Mohamed, J. Enzyme Inhib. Med. Chem. 37 (2021) 299–314.

[35]   Ayman Abo Elmaaty, Khaled M. Darwish, Amani Chrouda, Amira A. Boseila, Mohamed A. Tantawy, Sameh S. Elhady, Afzal B. Shaik, Muhamad Mustafa, A.A.A. In Silico and In Vitro Studies for Benzimidazole Anthelmintics Repurposing as VEGFR-2 Antagonists: Novel Mebendazole-Loaded Mixed Micelles with Enhanced Dissolution and Anticancer Activity, ACS Omega. 7 (2022) 875−899.

[36]   Kai Dührkop, Markus Fleischauer, Marcus Ludwig, Alexander A. Aksenov, Alexey V. Melnik, Marvin Meusel, Pieter C. Dorrestein, J.R. and S.B. SIRIUS4: a rapid tool for turning tandem mass spectra into metabolite structure information, Nat Methods. 16 (2019).

[37]   J. Silva dos Santos, J.P. Gonçalves Cirino, P. de Oliveira Carvalho, M.M. Ortega, The Pharmacological Action of Kaempferol in Central Nervous System Diseases: A Review, Front. Pharmacol. 11 (2021). https://doi.org/10.3389/fphar.2020.565700.

[38]   J. Li, M. Sun, X. Cui, C. Li, Protective Effects of Flavonoids against Alzheimer's Disease: Pathological Hypothesis, Potential Targets, and Structure–Activity Relationship, Int. J. Mol. Sci. 23 (2022). https://doi.org/10.3390/ijms231710020.

[39]   M.C. Yin, Anti-glycative potential of triterpenes: A mini-review, Biomed. 2 (2012) 2–9. https://doi.org/10.1016/j.biomed.2011.12.001.

[40]   O. ANDERSEN, P.R.A.S. Electron Impact and Chemical Ionization Mass Spectra of Catechol Derivatives from Insect Cuticle, Biomed. Mass Spectrom. 7 (1980) 317–320.

[41]   Z. Ren, B. Nie, T. Liu, F. Yuan, F. Feng, Y. Zhang, W. Zhou, X. Xu, M. Yao, F. Zhang, Simultaneous determination of coumarin and its derivatives in tobacco products by liquid chromatography-tandem mass spectrometry, Molecules. 21 (2016). https://doi.org/10.3390/molecules21111511.

[42]   R.F. Consiglio, Recent Applications ofMass Spectrometry in the Study of Grape andWine Polyphenols, ISRN Spectrosc. (2013) 45. http://dx.doi.org/10.1155/2013/813563.

[43]   G.H. Jang et al., Characterization and quantification of flavonoid glycosides in the Prunus genus by UPLC-DAD- QTOF/MS, Saudi J. Biol. Sci. 25 (2018) 1622–1631.

[44]   F. Imperato, Kaempferol and Quercetin 3-O-(2″,3″-di-O-p-coumaroyl)-Glucosides from Pteris vittata, Am. Fern Soc. 93 (2003) 157–160.

[45]   N. V. Petrova, A.A. Chernonosov, V. V. Koval, V.Y. Andreeva, A.S. Erst, A.A. Kuznetsov, M.S. Kulikovskiy, W. Wang, S.X. Yu, V.A.

Kostikova, LC–HRMS for the Identification of Quercetin and Its Derivatives in Spiraea hypericifolia (Rosaceae) and Anatomical Features of Its Leaves, Plants. 12 (2023). https://doi.org/10.3390/plants12020381.

[46]   A.F.G. da Cruz, A.C.C. Reis, J.A.C. Sousa, L.B.A. Vaz, B. de Mello Silva, C.L. de Brito Magalhães, M. Kohlhoff, A.B. de Oliveira, G.C. Brandão, High-Resolution Mass Spectrometry Identification and Characterization of Flavonoids from Fridericia chica Leaves Extract with Anti-Arbovirus Activity, Molecules. 27 (2022). https://doi.org/10.3390/molecules27186043.

[47]   Pal I. Holm, Per Magne Ueland, Gry Kvalheim, E.A.L. Determination of Choline, Betaine, and Dimethylglycine in Plasma by a High-Throughput Method Based on Normal-Phase Chromatography–Tandem Mass Spectrometry, Clin. Chem. 49 (2003) 286–294.

[48]   Sherifa Fahmy Moustafa, Rabab Mahrous Abdou, N.D.E.-T. and A.M.E. Metabolites Profiling of Pouteria Campechiana (Kunth) Baehni Different Organs Using UPLC-PDA-MS and its Biological Activities, Egypt. J. Chem. 66 (2023) 167–176.

[49]   B. Rehbock, D. Gansser, R.G. Berger, Analysis of oxylipins by high-performance liquid chromatography with evaporative light-scattering detection and particle beam-mass spectrometry, Lipids. 32 (1997) 1003–1010. https://doi.org/10.1007/s11745-997-0130-0.

[50]   C. Gravina, M. Fiorentino, M. Formato, M.T. Pecoraro, A. Stinca, S. Pacifico, A. Esposito, S. Piccolella, LC-HR / MS Analysis of Lipophilic Extracts from Source in Cosmeceuticals, Molecules. 27 (2022). https://doi.org/10.3390/molecules27248905.

[51]   C. S. R. Freire, A.J.D.S. and C.P.N.Identification of New Hydroxy Fatty Acids and Ferulic Acid Esters in the Wood of Eucalyptus globulus, Holzforschung. 56 (2002) 143–149.

[52]   R. Ghiulai, M. Mioc, R. Racoviceanu, A. Prodea, A. Milan, D. Coricovac, C. Dehelean, Ş. Avram, A.D. Zamfir, C.V.A. Munteanu, V. Ivan, C. Şoica, Structural Investigation of Betulinic Acid Plasma Metabolites by Tandem Mass Spectrometry, Molecules. 27 (2022). https://doi.org/10.3390/molecules27217359.

[53]   A.S. Jérémy Jacob, Jean-Robert Disnar, Mohammed Boussafir, Ana Luiza Spadano Albuquerque, Contrasted distributions of triterpene derivatives in the sediments of Lake Caçó reflect paleoenvironmental changes during the last 20,000 yrs in NE Brazil., Org. Geochem. 38 (2007) 180–197.

[54]   H. Takahashi, Y. Shimabukuro, D. Asakawa, S. Yamauchi, S. Sekiya, S. Iwamoto, M. Wada, K. Tanaka, Structural Analysis of

_____

_____

Phospholipid Using Hydrogen Abstraction Dissociation and Oxygen Attachment Dissociation in Tandem Mass Spectrometry, Anal. Chem. 90 (2018) 7230–7238.
https://doi.org/10.1021/acs.analchem.8b00322.

[55]   Á. Kuki, T. Nagy, M. Hashimov, S. File, M. Nagy, M. Zsuga, S. Kéki, Mass spectrometric characterization of epoxidized vegetable oils, Polymers (Basel). 11 (2019).
https://doi.org/10.3390/polym11030394.

[56]   K.S. Tamotsu Tanaka, Hideki Tsutsui, Kaoru Hirano, Tohru Koike, Akira Tokumura, Quantitative analysis of lysophosphatidic acid by time-of-flight mass spectrometry using a phosphate-capture molecule, J. Lipid Res. 45 (2004) 2145–2150.

[57]   National Center for Biotechnology Information."PubChem Compound Summary for CID 52924174, 1-pentadecanoyl-2-(13Z,16Z-docosadienoyl)-glycero-3- phosphoethanolamine" PubChem,
https://pubchem.ncbi.nlm.nih.gov/compound/529241 74. Accessed 16 August, 2023.

_____